Research Article

Fast Response Ammonia Gas Sensor Based on SnO_2 Nanoporous Synthesized By the Simple Heat-Up Method

Pitchanunt Chaiyo*

Received: 27 April 2023
Revised: 6 June 2023
Accepted: 8 June 2023

ABSTRACT

This paper investigated the electrical and gas-sensing properties of SnO_2 nanoporous synthesized via the simple heat-up method. The I-V characteristics of the SnO_2 nanoporous revealed Ohmic contact materials. The SnO_2 nanoporous sensor was tested upon exposure to 50 ppm ammonia gas at 250 °C. It showed an immediate response to ammonia with a recovery time of 200 s in the first cycle. Additionally, the SnO_2 nanoporous sensor was tested for its response to ammonia gas at concentrations ranging from 10 ppm to 90 ppm at a temperature of 250 °C. The results indicated that the SnO_2 nanoporous sensor responded to ammonia gas at low concentrations, even as low as 10 ppm. Furthermore, the relative response value of the SnO_2 nanoporous sensor demonstrated an increase in relative response value with increasing NH_3 concentration.

Keywords: SnO_2, Nanoporous, Heat-up method, Ammonia sensors, Gas sensor

Faculty of Sports and Health Science, Thailand National Sports University Sisaket Campus, Sisaket 33000, Thailand

*Corresponding author, email: Pitchanunt.chaiyo@gmail.com

Introduction

Currently, semiconductor metal oxide gas sensors, especially nanostructured metal oxides, have gained much attention from research communities due to their properties, such as high response, fast response and recovery time, room temperature operation, and low cost [1–4]. The most popular semiconductor metal oxide gas sensor is tin dioxide. Tin dioxide (SnO_2) is an N-type semiconductor with a stable wide bandgap of 3.6 eV [5]. SnO_2 nanostructured material has been researched for its ability to detect various gases, including nitrogen dioxide (NO_2), formaldehyde gas (HCHO), carbon dioxide (CO_2), carbon monoxide (CO), hydrogen sulfide (H_2S), ammonia (NH_3), and ethanol, among others [6–11]. However, tin dioxide nanomaterials can be synthesized by using various methods such as thermal evaporation, chemical vapor deposition (CVD), physical vapor evaporation (PVD), sol-gel, hydrothermal, atomic layer deposition (ALD), microwave-assisted, precipitation, and electrospinning [6,12–18]. These methods have their advantages and disadvantages for synthesizing SnO_2 nanomaterials. The advantages of these methods for the synthesis of SnO_2 nanomaterials include high crystallinity, selective deposition, and high purity. However, these methods can also have disadvantages such as high equipment costs, complexity, high temperatures, high-pressure vessels, hazardous precursor gases, and long processing time [19]. One interesting method for synthesizing semiconductor nanomaterials is the heat-up method because it is relatively simple, uncomplicated, low-cost, and cost-effective [20, 21]. Moreover, it can produce various nanostructured materials, including oxides, metals, and semiconductors. However, the heat-up method has the following limitations: temperature instability, difficulties with product reproducibility, and difficulties in controlling the size and shape [22, 23].

Ammonia gas is a toxic, colorless, odorous, and corrosive gas with the general chemical name of ammonia anhydrous. It is an inorganic substance with the molecular formula NH_3. Ammonia is used in various chemical industries, such as fertilizer production, petrochemical equipment, beverage production, the automotive industry, explosives, plastics, and pesticides. Ammonia is widely used in the refrigeration industry as a refrigerant for various products, including vegetable and fruit juices, soft drinks, breweries and wineries, meat processing, cold storage warehouses, and ice rinks for sports [24]. However, ammonia has highly toxic and corrosive properties that can harm the skin, eyes, throat, and lungs of those who inhale it. Therefore, it is crucial not to inhale it above the safe level, as it can cause life-threatening diseases. The Occupational Safety and Health Administration (OSHA) has set an acceptable exposure limit for ammonia to humans at 25 ppm for 8 hours and 35 ppm for 15 minutes [24, 25].

A research study on the detection of ammonia gas by using tin dioxide nanomaterials has been reported. Phuoc et al. synthesized SnO_2 porous nanofiber by using a facile electrospinning method and examined its response to H_2S gas at concentrations of 0.1-1 ppm and temperatures of 150 to 450 °C. The fabricated sensor demonstrated fast response and recovery times, with a gas response of 15.2 [26]. Shruthi et al. fabricated Ag:Y_2O_3–SnO_2 core-shell-based nanostructured sensor by using a simple slurry coating method. The Ag:Y_2O_3–SnO_2 sensor was tested for ammonia concentrations ranging from 1 ppm

to 100 ppm at room temperature. The sensor exhibited rapid response (2 s) and recovery times (8 s), with the highest response [27].

In this study, we present the SnO_2 nanoporous materials synthesized using a simple heat-up method at temperatures of 110 °C and 240 °C. Additionally, we report on the dynamic response and recovery cycle of SnO_2 nanoporous when exposed to NH_3 gas concentrations of 50 ppm at a temperature of 250 °C. To confirm the results of this study, we continued to observe the dynamic response and recovery cycle of SnO_2 nanoporous when exposed to NH_3 gas concentrations ranging from 10 ppm to 90 ppm at a temperature of 250 °C.

Materials and Methods

Fabrication of SnO_2 nanoporous

The SnO_2 nanoporous were prepared by the heat-up method. Firstly, 3.102 g of Tin (IV) bis (acetylacetonate) dichloride and 2.069 g of 1,2-hexadecane-diol were added to dibenzyl ether (60 mL), which served as the solvent in a three-necked flask, as shown in Figure 1. Then, 6 mL of oleyl amine was added as a reducing and growth agent to regulate the crystal growth. After that, the solvent in a three-necked flask was heated at 110 °C for 30 min under oxygen-free vacuum conditions and then heated to 240 °C for 30 min. Next, the sample was washed and centrifuged three times with ethanol. Finally, the sample was dispersed in deionized (DI) water [20, 21].

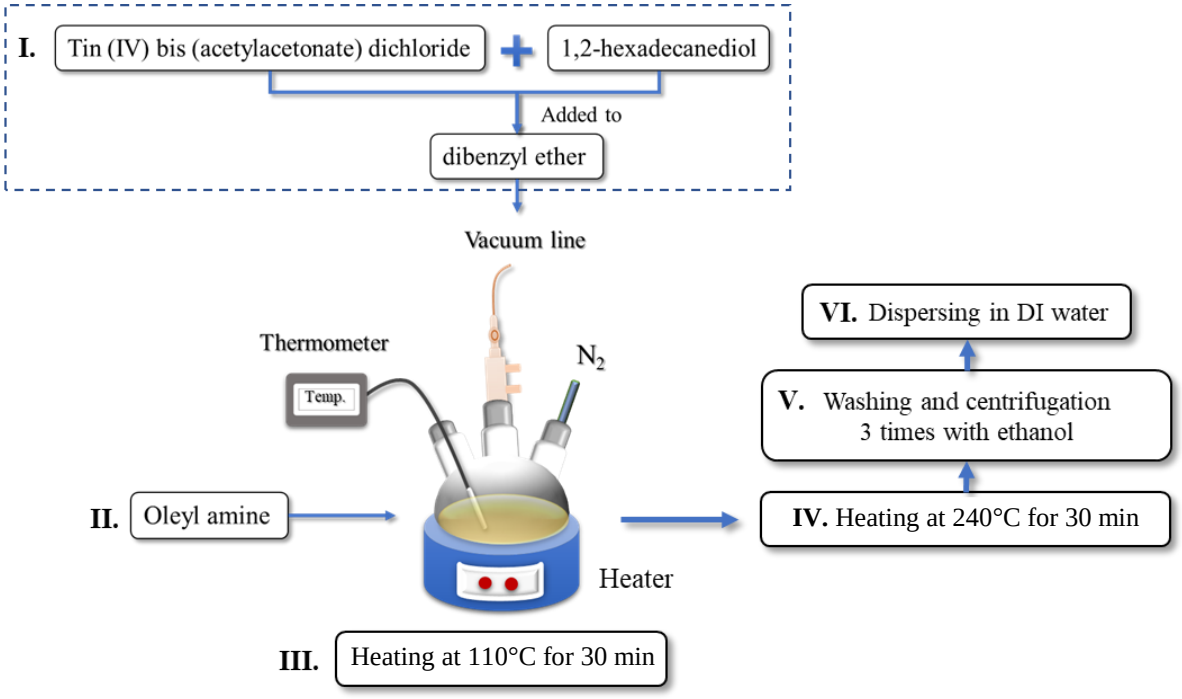

Figure 1 Schematic of SnO_2 nanoporous preparation by the heat-up method.

Characterization of SnO_2 nanoporous

The morphology of the SnO_2 nanoporous was investigated by using scanning electron microscopy (SEM, Hitachi S-4800). Then, the crystal structure of the sample was analyzed by using an

X-ray diffraction technique (XRD, Rigaku SmartLab High-Resolution X-ray Diffractometer (HR-XRD) using Cu Ka (λ = 1.5418 Å) at 45 kV and 200 mA). X-ray photoelectron spectroscopy (XPS, K-alpha, Thermo Scientific using conventional monochromatic Al Kα radiation (hν = 1486.6 eV) with θ = 0° (normal emission) and a pass energy of 50 eV was used to examine the sample components.

Fabrication of SnO_2 nanoporous sensor

The synthesized SnO_2 nanoporous in DI water were dropped onto the interdigitated electrodes (IDE) electrode (Cr/Au, 3/70 nm) with a volume of 2 µl, as shown in Figure 2. Then, the sample was heated in an N_2 atmosphere for 3 minutes at 300 °C to improve ohmic contact.

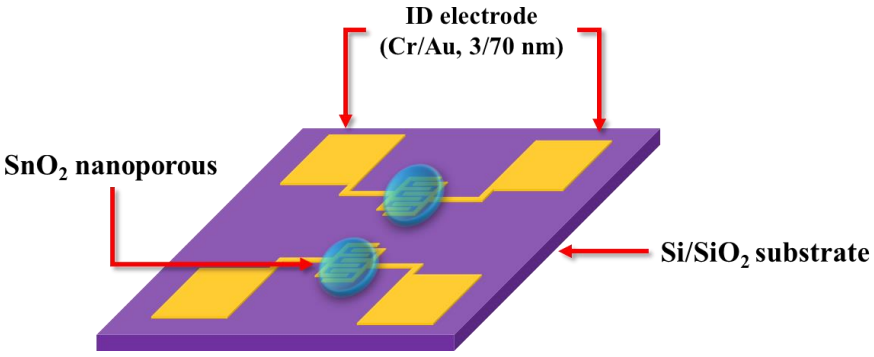

Figure 2 Schematic of SnO_2 nanoporous sensor fabrication.

Measurement of the electrical and gas-sensing properties

The electrical properties of the sample were measured in the range of −3 V to 3 V at temperatures of room temperature (RT) and 250 °C. The sensitivity of the SnO_2 nanoporous sensor was measured by using a Keithley-4200 semiconductor parameter analyzer at 250 °C. The sample's resistance, current, and response were examined by exposing them to NH_3 gas at concentrations of 50 ppm and different concentrations ranging from 10-90 ppm. The heater and gas flow were controlled by a Hanyoung Nux PX7 and a Victor SR312, respectively. The relative response can be calculated via the following equation (1)

$$RH = \frac{|R_a - R_g|}{R_a} \times 100\% \quad (1)$$

where RH is relative response, R_a is resistance in an air atmosphere, and R_g is resistance in an ammonia atmosphere [28].

Results and discussion

The sample's surface morphology was investigated using the SEM technique, as shown in Figure 3(a-b). The SEM images showed an area with a cracked porous structure at a magnification 4,000x (bar 1 µm) and 16,000x (bar 300 nm). Figure 3(c) shows high-magnification SEM images (magnification

30,000x, bar 200 nm). It can be seen that the surface morphology exhibits numerous pores in the SnO_2 materials, which greatly helps in improving the response of the gas sensor. However, the pore diameters vary in the range of 10-100 nm.

The crystal structure of the SnO_2 nanoporous was investigated by the X-ray diffractometer technique, as shown in Figure 4. The XRD pattern (Figure 4) shows the SnO_2 phase at planes of (110), (101), and (211), which correspond to the peaks of 26.10, 33.55, and 51.35, respectively. Moreover, the results indicated a tetragonal crystal system according to the JCPDS pattern (41-1445) [29, 30]. Additionally, the XRD pattern of the sample showed low intensity and small peaks. As a result, the SnO_2 nanoporous were relatively low in crystallinity. The atomic percentages of the sample were investigated by the X-ray photoelectron spectroscopy technique, as shown in Table 1. The atomic percentages of Sn, O, and C were 18.67, 45.33, and 36.00, respectively. Therefore, the ratio of Sn and O atoms was approximately 1:2.

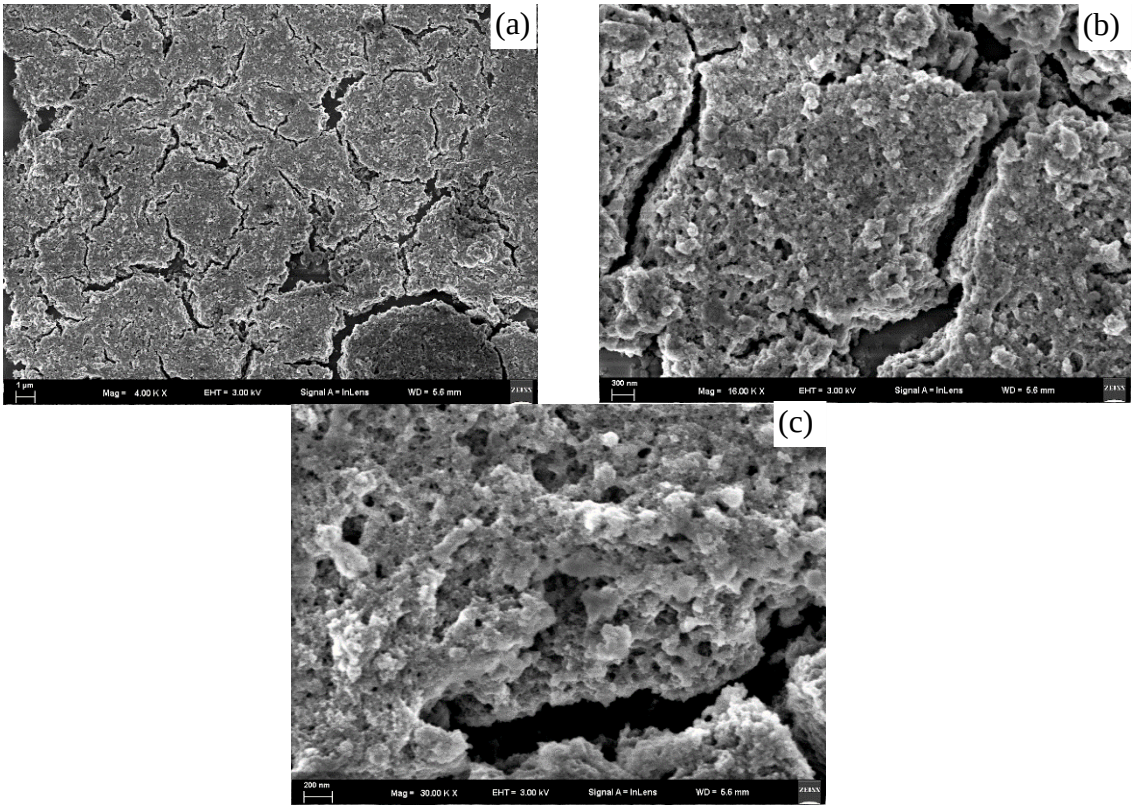

Figure 3 (a) Low and (b) high magnification SEM images of the SnO_2 nanoporous.

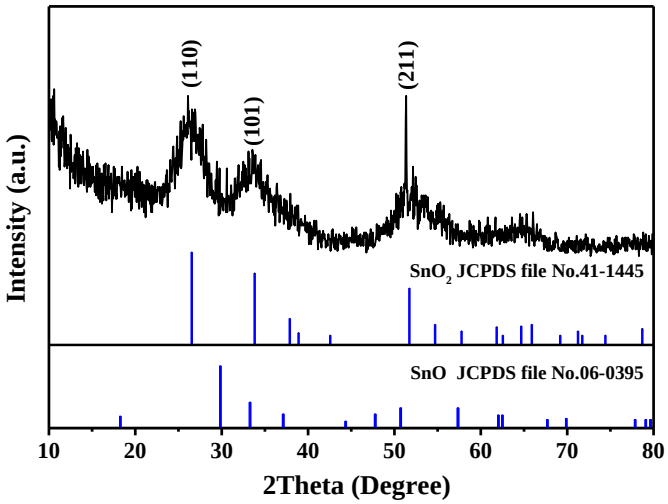

Figure 4 XRD pattern of the SnO_2 nanoporous with JCPDS file No.41-1445.

Table 1 Atomic percent of the SnO_2 nanoporous

Elements	Atomic percent (%)
Sn 3d	18.67
O 1s	45.33
C 1s	36.00

Figure 5 shows the XPS patterns of the SnO_2 nanoporous with elemental descriptions. The survey spectrum of the SnO_2 nanoporous (Figure 5(a)) demonstrated that the sample consisted of peaks from the elements Sn, O, and C. Figure 5(b) shows the peaks of the Sn element. The Sn 3d symmetrical peaks appeared at 495.1 eV and 486.7 eV, corresponding to Sn $3d_{3/2}$ and Sn $3d_{5/2}$, respectively. Moreover, the binding energy separation between Sn $3d_{3/2}$ and Sn $3d_{5/2}$ peaks was 8.4 eV. This result could be attributed to the binding energy of the Sn^{4+} and was consistent with previous reports [31, 32]. Figure 5(c) demonstrates the O element peaks, with O 1s appearing at 533.1 eV, 531.8 eV, and 530.6 eV corresponding to adsorbed oxygen (O_{ads}), defective oxygen (O_v) and lattice oxygen (O_L), respectively [32].

Figure 6 demonstrates the I-V characteristic curves of the SnO_2 nanoporous measured at temperatures of RT (red line) and 250 °C (black line). The results showed linear relations and indicated ohmic contact materials [33]. In addition, the resistance values were calculated via the I-V linear relation slope. Therefore, the resistance values of the SnO_2 nanoporous were 6.54×10^4 MΩ and 2.45×10^2 MΩ measured at temperatures of RT and 250 °C, respectively. The results suggested that the electrical conductivity of the SnO_2 nanoporous was greater when measured at 250°C than when measured at RT.

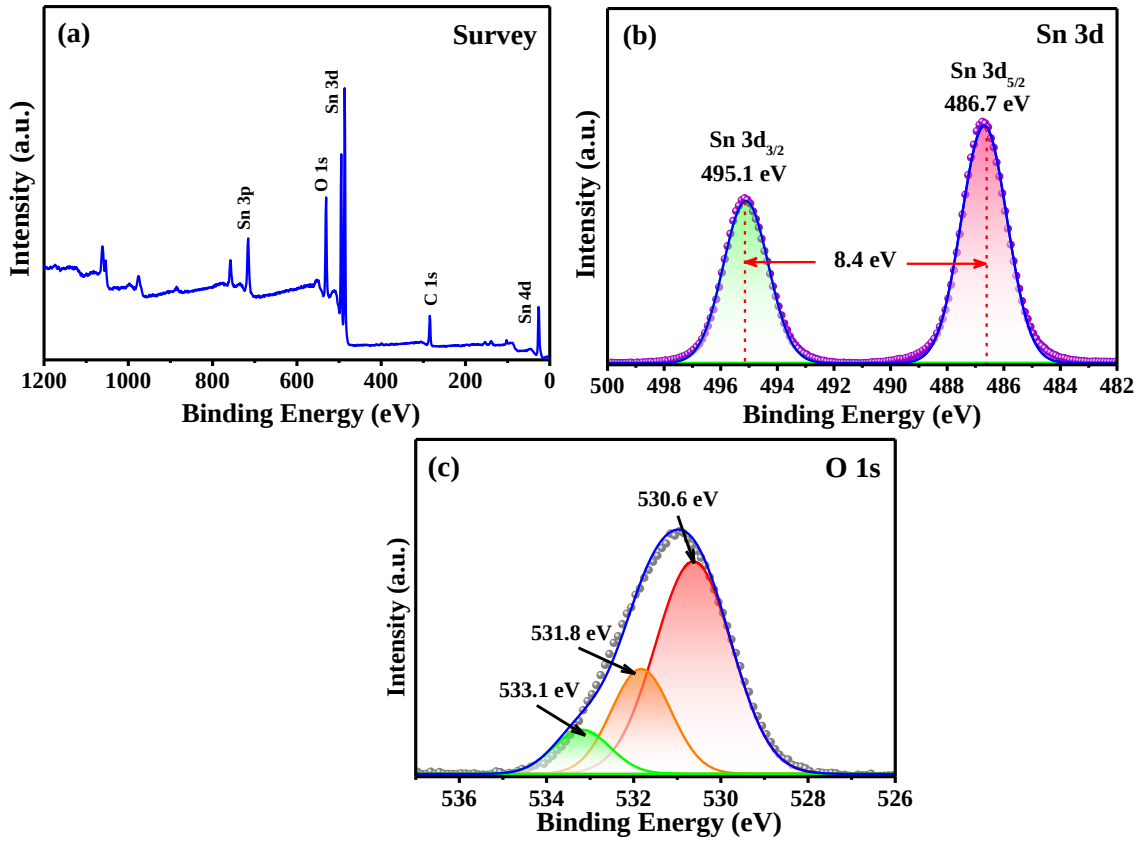

Figure 5 XPS patterns of the as-synthesized SnO_2 nanoporous: (a) survey spectrum and high-resolution spectra of (b) Sn 3d, (c) O 1s, and (d) C 1s.

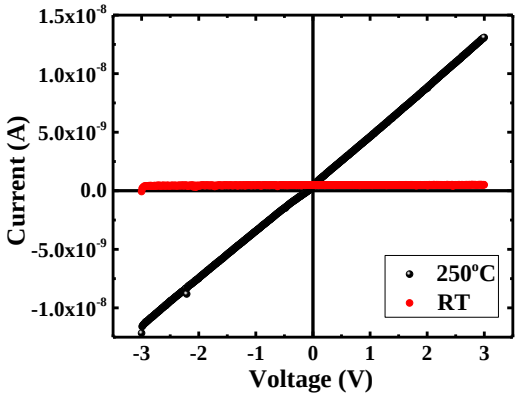

Figure 6 I-V curves of SnO_2 nanoporous measured at RT and 250 °C.

Figure 7(a) shows the dynamic response and recovery time cycles of the SnO_2 nanoporous sensor upon exposure to NH_3 gas with a concentration of 50 ppm at 250 °C. The response and recovery test cycle were repeated two times. The results unambiguously showed that the two cycles' response values differed. The first cycle had an immediate response to the NH_3 gas, with a response of about 60%. Then, the response value of the first cycle decreased to about 40%. According to Figure 7(b), the

first cycle recovery time (t_{rec}) was 200 s. The high-resolution second response cycle of the SnO_2 nanoporous sensor (Figure 7(c)) showed a slow response time, with a response time value (t_{res}) of approximately 80 s, which is clearly seen as a bend in the response time curve. In addition, the recovery time (t_{rec}) of this cycle was 300 s. This result showed that the sensor had a slower response to ammonia gas and a longer recovery time.

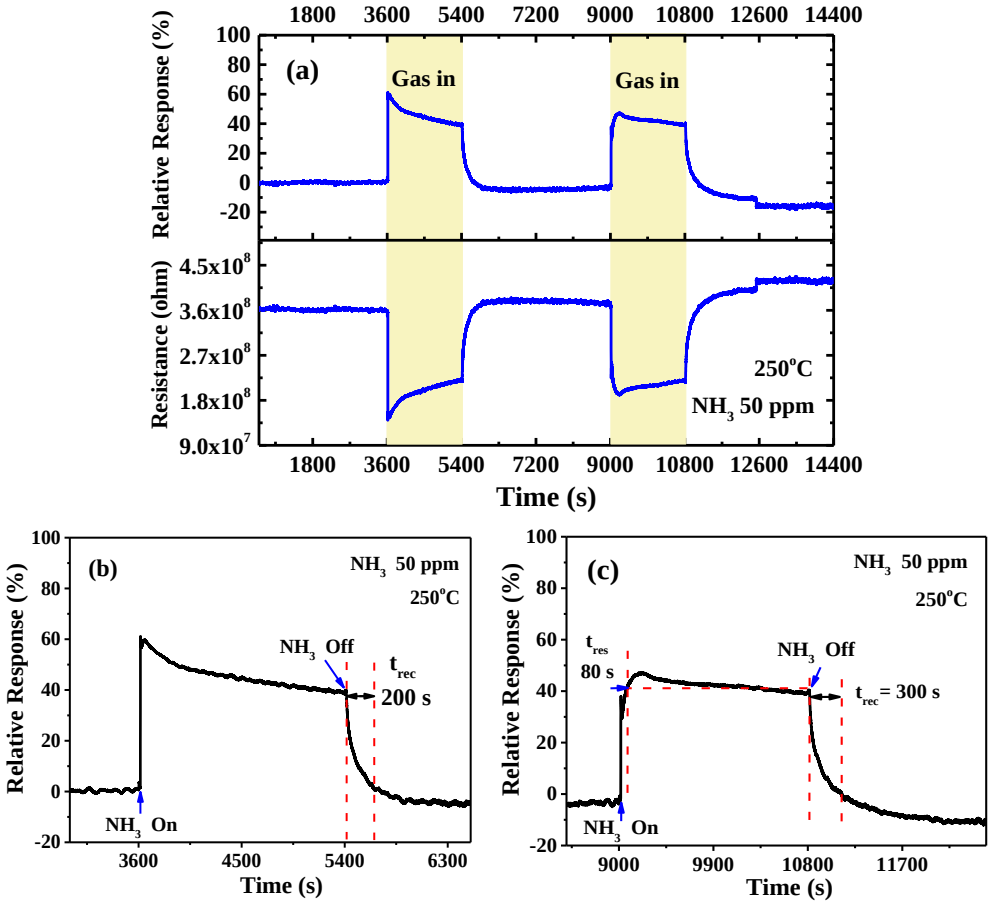

Figure 7 (a) Relative response curves of SnO_2 nanoporous sensor upon exposure to NH_3 gas concentration of 50 ppm at 250°C. The high-resolution response of (b) first and (c) second cycle.

However, the SnO_2 nanoporous sensors were tested for their response to NH_3 gas at concentrations ranging from 10 ppm to 90 ppm at 250 °C, as shown in Figure 8, and the response and recovery time of the SnO_2 nanoporous sensor demonstrated an increase in response time with increasing NH_3 concentration [34, 35]. According to Figure 8, the SnO_2 nanoporous sensor had the lowest response at a concentration of 10 ppm and greatest at a concentration of 90 ppm. Furthermore, the response and recovery cycles of the SnO_2 nanoporous sensor at concentrations ranging from 10 ppm to 50 ppm were similar. When the response value reached its maximum value, it gradually decreased. However, the response and recovery cycles of the SnO_2 nanoporous sensors at NH_3 concentrations ranging from 70 ppm to 90 ppm exhibited a similar curve bending in the response time.

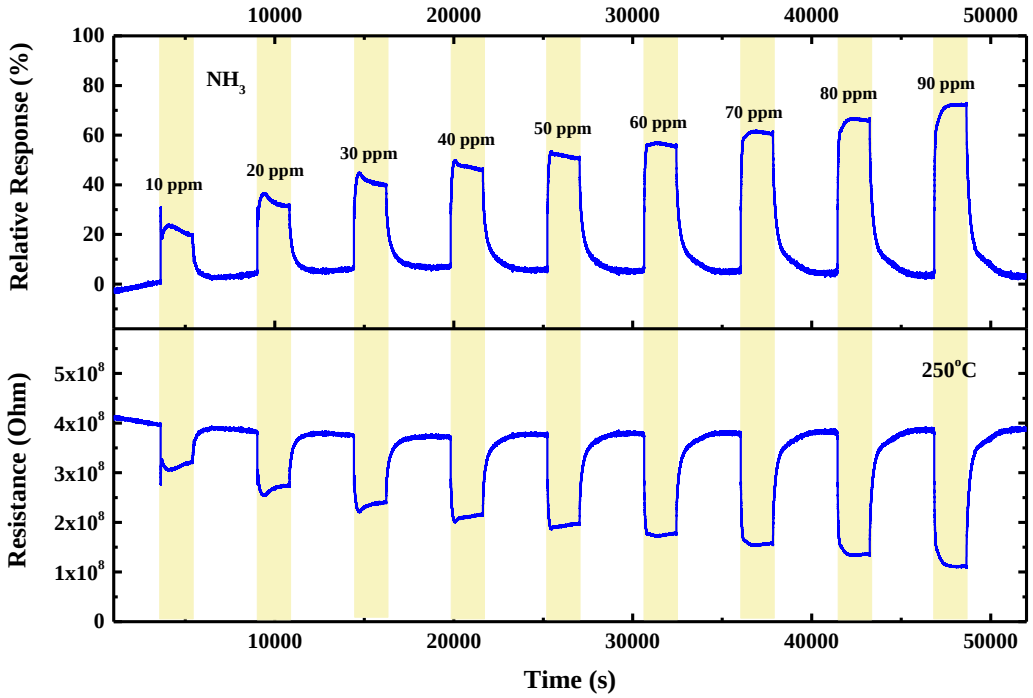

Figure 8 The response and recovery cycles of the SnO_2 nanoporous sensor were investigated upon exposure to NH_3 gas in various concentrations ranging from 10 ppm to 90 ppm at 250 °C.

Consequently, their response to NH_3 gas reached a stable state with response values of approximately 61%, 66%, and 71%, corresponding to concentrations of 70 ppm, 80 ppm, and 90 ppm, respectively. Moreover, the response and recovery cycle of the SnO_2 nanoporous sensor at an NH_3 gas concentration of 60 ppm exhibited the most stable response values compared to the cycles at other concentrations. This cycle showed no bending in the response time and maintained a constant response value during the presence and absence of ammonia gas in the chamber. Therefore, the results suggested that the SnO_2 nanoparticle sensor was suitable for detecting ammonia gas at a concentration of 60 ppm. The response remained stable for 1800 s with a response value of approximately 56%.

Figure 9 illustrates the gas sensor mechanism of the SnO_2 nanoporous sensor in an ammonia atmosphere at 250 °C. The chemical reaction of the SnO_2 nanoporous sensor in air and ammonia atmospheres can be described via the following equation (2-8), respectively [28, 34, 35].

$$O_{2(ads)} \rightleftharpoons O_{2(ads)} \quad (2)$$

$$O_{2(ads)} + e^- \rightleftharpoons O^-_{2(ads)} \quad (T < 100\ ^oC) \quad (3)$$

$$O^-_{2(ads)} + e^- \rightleftharpoons 2O^-_{(ads)} \quad (100^oC \leq T \leq 300^oC) \quad (4)$$

$$O^-_{(ads)} + e^- \rightleftharpoons O^{2-}_{(ads)} \quad (T > 300\ ^oC) \quad (5)$$

$$2NH_3 + 3O^-_{(ads)} \rightleftharpoons N_2 + 3H_2O + 3e^- \quad (6)$$

$$2NH_3 + 4O^-_{(ads)} \rightleftharpoons N_2O + 3H_2O + 4e^- \quad (7)$$

$$2NH_3 + 5O^-_{(ads)} \rightleftharpoons 2NO + 3H_2O + 5e^- \quad (8)$$

In air, the initial resistance of the SnO_2 nanoporous was high because the oxygen at the surface area of the SnO_2 nanoporous was capturing the nearly free electrons, as shown in the reaction equation (4). Therefore, the surface area of the SnO_2 nanoporous had a low free electron concentration. Additionally, the oxygen atoms become oxygen ions. As a result, the space charge region width became wider. However, when the surface area of the SnO_2 nanoporous was exposed to ammonia gas, the space charge region width became narrow because the oxygen ions reacted with ammonia gas, as shown in the reaction equation (6-7). This reaction resulted in free electrons from the previous reaction being released onto the surface area of the SnO_2 nanoporous, causing the resistance of the SnO_2 nanoporous to be lower than the initial resistance value [5, 36-38].

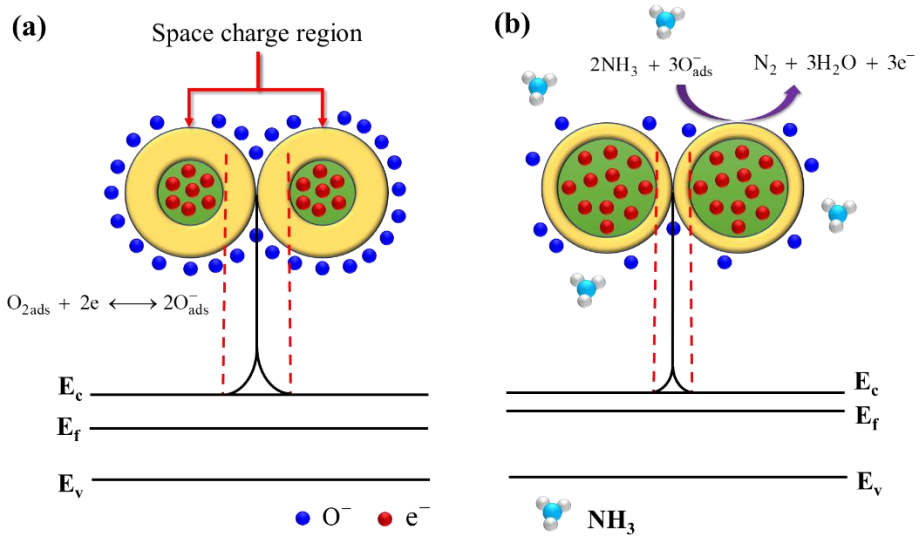

Figure 9 Schematic of the sensing mechanism of SnO_2 nanoporous (a) in air and (b) NH_3 atmospheres.

Conclusions

In summary, SnO_2 nanoporous were successfully synthesized by using the simple heat-up method. The surface morphology of the as-synthesized sample was investigated by using SEM techniques, demonstrating a cracked, porous structure for the SnO_2 nanoporous. The crystal structure of the SnO_2 nanoporous was analyzed by using XRD techniques, revealing a tetragonal crystal structure for SnO_2. The I-V characteristics of the SnO_2 nanoporous exhibited ohmic contact materials. The SnO_2 nanoporous sensor showed a fast response and recovery time when exposed to NH_3 gas at a concentration of 50 ppm and a temperature of 250 °C. Additionally, this sensor responded to NH_3 gas at low concentrations of 10 ppm, with the response value increasing as the NH_3 concentration increased.

Acknowledgments

This work was supported by the Thin Film Materials Research Center at the Korea Research Institute of Chemical Technology and Thailand National Sports University Sisaket Campus. The authors would like to thank them for the financial support and research facility. Finally, the authors would like

to especially thank Assoc. Prof. Dr. Supakorn Pukird, Dr. Ki-Seok An, and Dr. Yeong Min Kwon for helping and giving advice.

References

1. Zhen YX, Song BY, Liu WX, Ye JX, Zhang XF, Deng ZP, et al. Ultra-high response and low temperature NO_2 sensor based on mesoporous SnO_2 hierarchical microtubes synthesized by biotemplating process. Sens Actuators B Chem. 2022;363:131852.
2. Song BY, Li C, Lv MS, Zhang XF, Deng ZP, Xu YM, et al. Biotemplate-inherited porous SnO_2 monotubes with oxygen vacancies for ultra-high response and fast detection of nitric oxide at low temperature. Sens Actuators B Chem. 2023; 387:133811.
3. Yan J, Guo X, Zhu Y, Song Z, Lee LYS. Solution-processed metal doping of sub-3 nm SnO_2 quantum wires for enhanced H_2S sensing at low temperature. J Mater Chem A. 2022;10:15657.
4. Zappa D, Galstyan V, Kaur N, Arachchige M, Sisman O, Comini E. Metal oxide-based heterostructures for gas sensors-a review. Anal Chim Acta. 2018;1039:1-23.
5. Zhang L, Tong R, Ge W, Guo R, Shirsath SE, Zhu J. Facile one-step hydrothermal synthesis of SnO_2 microspheres with oxygen vacancies for superior ethanol sensor. J Alloys Compd. 2020;814:152266.
6. Bai M, Chen M, Li X, Wang Q. One-step CVD growth of ZnO nanorod/SnO_2 film heterojunction for NO_2 gas sensor. Sens Actuators B Chem. 2022;373:132738.
7. Li N, Fan Y, Shi Y, Xiang Q, Wang X, Xu J. A low temperature formaldehyde gas sensor based on hierarchical SnO/SnO_2 nano-flowers assembled from ultrathin nanosheets: Synthesis, sensing performance and mechanism. Sens Actuators B Chem. 2019;294:106-15.
8. Panday M, Upadhyay GK, Purohit LP. Sb incorporated SnO_2 nanostructured thin films for CO_2 gas sensing and humidity sensing applications. J Alloys Compd. 2022;904:164053.
9. Jian KS, Chang CJ, Wu JJ, Chang YC, Tsay CY, Chen JH, et al. High response CO sensor based on a polyaniline/SnO_2 nanocomposite. Polymers. 2019;11:184.
10. Kumar A, Shringi AK, Kumar M. RF sputtered CuO anchored SnO_2 for H_2S gas sensor. Sens Actuators B Chem. 2022;370:132417.
11. Sun X, Chen T, Liang Y, Zhang C, Zhai S, Sun J, et al. Enhanced sensitivity of SAW based ammonia sensor employing GO-SnO_2 nanocomposites. Sens Actuators B Chem. 2023;375:132884.
12. Duoc VT, Hung CM, Nguyen H, Duy NV, Hieu NV, Hoa ND, et al. Room temperature highly toxic NO_2 gas sensors based on rootstock/scion nanowires of SnO_2/ZnO, ZnO/SnO_2, SnO_2/SnO_2 and, ZnO/ZnO. Sens Actuators B Chem. 2021;348:130652.
13. Sisman O, Kaur N, Sberveglieri G, Núñez-Carmona E, Sberveglieri V, Comini E. UV-enhanced humidity sensing of Chitosan–SnO_2. Nanomaterials (Basel). 2020;10(2):329.

14. Khan D, Rehman A, Rafiq MZ, Khan AM, Ali M. Improving the optical properties of SnO_2 nanoparticles through Ni doping by sol- gel technique. Curr Res Green Sustain Chem. 2021;4:100079.
15. Hsu SH, Liao HT, Chen RS, Chiu SC, Tsai FY, Lee MS, et al. The influence on surface characteristic and biocompatibility of nano-SnO_2-modified titanium implant materials using atomic layer deposition technique. J Formos Med Assoc. 2023;122:230-8.
16. Gaber A, Attia SY, Salem AMS, Mohamed SG, El-Hout SI. Microwave-assisted fabrication of SnO_2 nanostructures as electrode for high- performance pseudocapacitors. J Energy Storage. 2023;59:106358.
17. Naz S, Javid I, Konwar S, Surana K, Singh PK, Sahni M, et al. A simple low cost method for synthesis of SnO_2 nanoparticles and its characterization. SN Appl Sci. 2020;2:975.
18. Zhang J, Ma S, Wang B, Pei S. Preparation of composite SnO_2/CuO nanotubes by electrospinning and excellent gas selectivity to ethanol. Sens Actuators A Phys. 2021;332(1):113090.
19. Kong Y, Li Y, Cui X, Su L, Ma D, Lai T, et al. SnO_2 nanostructured materials used as gas sensors for the detection of hazardous and flammable gases: a review. Nano Mater Sci. 2022;4(4):339-350.
20. Pramata AD, Suematsu K, Quitain AT, Sasaki M, Kida T. Synthesis of highly luminescent SnO_2 Nanoporous: Analysis of their defect-related photoluminescence using polyoxometalates as quenchers. Adv Funct Mater 2018;28:1704620.
21. Purbia R, Kwon YM, Kim HD, Lee YS, Shin H, Baik M. Zero-dimensional heterostructures: N-doped graphene dots/SnO_2 for ultrasensitive and selective NO_2 gas sensing at low temperatures. J Mater Chem. A. 2020;8:11734.
22. Kulpa-Greszta M, Tomaszewska A, Dziedzic A, Pązik R. Rapid hot-injection as a tool for control of magnetic nanoparticle size and morphology. RSC Adv. 2021;11:20708-19.
23. Muro-Cruces J, Roca AG, López-Ortega A, Fantechi E, del-Pozo-Bueno D, Estrade S, et al. Precise size control of the growth of Fe_3O_4 nanocubes over a wide size range using a rationally designed one-pot synthesis. ACS Nano. 2019;13(7):7716-28.
24. Kwak D, Lei Y, Maric R. Ammonia gas sensors: a comprehensive review. Talanta. 2019;204:713-30.
25. Verma A, Kumar P, Singh VK, Mishra VN, Prakash R. Introduction of graphene oxide nanosheets in self-oriented air-stable poly(3-hexylthiophene-2,5-diyl) to enhance the ammonia gas sensing of a p-channel thin film transistor. Sens Actuators B Chem. 2023;385:133661.
26. Phuoc PH, Hung CM, Toan NV, Duy NV, Hoa ND, Hieu NV. One- step fabrication of SnO_2 porous nanofiber gas sensors for sub- ppm H_2S detection. Sens Actuators B Physical. 2020;303:111722.
27. Shruthi J, Jayababu N, Reddy MVR. Ag:Y_2O_3–SnO_2 core-shell-based nanostructured sensor for achieving high ammonia sensing performance. Appl Phys A Mater Sci Process. 2022;128:999.

28. Krishna KG, Parne S, Pothukanuri N, Kathirvelu V, Gandi S, Joshi D. Nanostructured metal oxide semiconductor-based gas sensors: A comprehensive review. Sens Actuators A Phys. 2022;341:113578.
29. Mahjouri S, Kosari-Nasab M, Mohajel Kazemi E, Divband B, Movafeghi A. Effect of Ag-doping on cytotoxicity of SnO_2 nanoparticles in tobacco cell cultures. J Hazard Mater. 2020;381:121012.
30. Li J, Chen C, Li J, Li S, Dong C. Synthesis of tin-glycerate and it conversion into SnO_2 spheres for highly sensitive low-ppm-level acetone detection. J Mater Sci Mater Electron. 2020;31:16539–47.
31. He T, Liu W, Lv T, Ma M, Liu Z, Vasiliev A, et al. MXene/SnO_2 heterojunction based chemical gas sensors. Sens Actuators B Chem. 2021;329:129275.
32. Choi PG, Izu N, Shirahata N, Masuda Y. SnO_2 Nanosheets for selective alkene gas sensing. ACS. Nano Mater. 2019;2:1820-27.
33. Soussi I, Garmim T, Karzazi O, Rmili A, Bachiri AE, Louardi A, et al. Effect of (Co, Fe, Ni) doping on structural, optical and electrical properties of sprayed SnO_2 thin film. Surf Interfaces. 2020;19:100467.
34. Maheswari S, Karunakaran M, Kasirajan K, Chandrasekar LB, Boomi P. Yttrium-Substituted SnO_2 thin films and its gas sensing activity against NH_3 gas: characterization and sensitivity evaluation. Sens Actuators A Phys. 2020;315:112303.
35. Yang T, Zhang X, Shiu BC, Lou CW, Lin JH, Li TT. Wearable smart yarn sensor based on ZnO/SnO_2 heterojunction for ammonia detecting. J Mater Sci. 2022;57:21946-59.
36. Zhang N, Fan Y, Lu Y, Li C, Zhou J, Li X, et al. Synthesis of au-decorated SnO_2 crystallites with exposed (221) facets and their enhanced acetylene sensing properties. Sens Actuators B Chem. 2020;307:127629.
37. Kang X, Deng N, Yan Z, Pan Y, Sun W, Zhang Y. Resistive-type VOCs and pollution gases sensor based on SnO_2: a review. Mater Sci Semicond Process. 2022;138:106246.
38. Masuda Y. Recent advances in SnO_2 nanostructure based gas sensors. Sens Actuators B Chem. 2022;364:131876.